

# A SAMPLE OF QUASARS WITH STRONG NITROGEN EMISSION LINES FROM THE SLOAN DIGITAL SKY SURVEY

LINHUA JIANG<sup>1</sup>, XIAOHUI FAN<sup>1</sup>, AND M. VESTERGAARD<sup>2</sup>

*Draft version February 28, 2008*

## ABSTRACT

We report on 293 quasars with strong N IV]  $\lambda$ 1486 or N III]  $\lambda$ 1750 emission lines (rest-frame equivalent width  $> 3 \text{ \AA}$ ) at  $1.7 < z < 4.0$  selected from the Sloan Digital Sky Survey (SDSS) Fifth Data Release. These nitrogen-rich (N-rich) objects comprise  $\sim 1.1\%$  of the SDSS quasars. The comparison between the N-rich quasars and other quasars shows that the two quasar subsets share many common properties. We also confirm previous results that N-rich quasars have much stronger Ly $\alpha$  and N V  $\lambda$ 1240 emission lines. Strong nitrogen emission in all ionization states indicates high overall nitrogen abundances in these objects. We find evidence that the nitrogen abundance is closely related to quasar radio properties. The radio-loud fraction in the N III]-rich quasars is 26% and in the N IV]-rich quasars is 69%, significantly higher than  $\sim 8\%$  measured in other quasars with similar redshift and luminosity. Therefore, the high nitrogen abundance in N-rich quasars could be an indicator of a special quasar evolution stage, in which the radio activity is also strong.

*Subject headings:* galaxies: active — quasars: emission lines — quasars: general

## 1. INTRODUCTION

Quasars with prominent nitrogen emission lines at 1486  $\text{\AA}$  or 1750  $\text{\AA}$  are rare. A well known example is Q0353-383, a luminous quasar showing strong N IV]  $\lambda$ 1486, N III]  $\lambda$ 1750, and N V  $\lambda$ 1240 emission lines (Osmer & Smith 1980; Baldwin et al. 2003). Baldwin et al. (2003) claimed that the unusual nitrogen emission in Q0353-383 is likely due to high metallicity in the broad line region of the quasar; the metallicity measured from line strength ratios involving N V, N IV], and N III] is  $\sim 15$  times the solar abundance.

The Sloan Digital Sky Survey (SDSS; York et al. 2000) provides statistically significant samples to study these nitrogen-rich (N-rich) quasars. From a sample of  $\sim 5600$  objects in the SDSS First Data Release Quasar Catalog (Schneider et al. 2003), Bentz et al. (2004) reported on 20 N-rich quasars in the redshift range  $1.6 < z < 4.1$ . The fraction of N-rich quasars in their sample is about 0.4%. By comparing with other quasars, they found that the N-rich quasars tend to have stronger Ly $\alpha$  emission lines, and stronger but narrower C IV  $\lambda$ 1549 and C III]  $\lambda$ 1909 emission lines. The two quasars with the strongest N IV] and N III] lines in the Bentz et al. (2004) sample have been studied in detail by Dhanda et al. (2007). Recently Glikman et al. (2007) discovered two quasars with strong N IV] lines from a sample of 23 faint quasars at  $3.7 < z < 5.1$ . They suspected that the high detection rate of N-rich quasars is due to the low luminosity and high redshift of the sample.

The number of known N-rich quasars is still small, and most of their properties remain unclear, such as the UV/optical continuum slopes, emission line strengths and widths, and central black hole masses, etc. In this paper, we present 293 N-rich quasars at  $z > 1.7$  selected from the SDSS Fifth Data Release (DR5) Quasar Catalog (Schneider et al. 2007). In § 2, we introduce our sample

selection. We measure various properties of these quasars and compare them with those of other SDSS quasars in § 3. A short summary is given in § 4. Throughout the paper we use a  $\Lambda$ -dominated flat cosmology with  $H_0 = 70 \text{ km s}^{-1} \text{ Mpc}^{-1}$ ,  $\Omega_m = 0.3$ , and  $\Omega_\Lambda = 0.7$  (Spergel et al. 2007). We use EW and FWHM to denote *rest-frame* equivalent width and full width at half maximum, respectively.

## 2. SAMPLE SELECTION

The SDSS is an imaging and spectroscopic survey using a dedicated wide-field 2.5m telescope (Gunn et al. 2006). The imaging is carried out in five broad bands, *ugriz*, spanning the range from 3000 to 10,000  $\text{\AA}$  (Fukugita et al. 1996); spectroscopy is performed using a pair of double spectrographs with coverage from 3800 to 9200  $\text{\AA}$ , and a resolution  $\lambda/\Delta\lambda$  of roughly 2000. The SDSS quasar survey spectroscopically targets quasars with  $i < 19.1$  at low redshift ( $z \leq 3$ ) and  $i < 20.2$  at high redshift ( $z \geq 3$ ). Quasar candidates are mostly selected in *ugri* and *griz* color space (Richards et al. 2002). An SDSS object is also considered to be a primary quasar candidate if it is located within  $2''$  of a radio source of the Faint Images of the Radio Sky at Twenty-cm survey (FIRST; Becker et al. 1995). The sample we use is from the SDSS DR5 Quasar Catalog. The catalog consists of 77,429 quasars with luminosities larger than  $M_i = -22$  (Schneider et al. 2007).

To find quasars with prominent N IV] or N III] emission lines, we searched 25,941 quasar spectra with  $i < 20.1$  in the redshift range  $1.7 < z < 4.0$ . The search was done by visual inspection of each spectrum. This step results in a sample of 380 N-rich quasar candidates. We then measured the rest-frame EW and FWHM for each detected N IV] or N III] line as follows. We estimate the local continuum by fitting a power-law to the spectra at both sides of the line. After subtraction of this continuum, a Gaussian profile is fitted to the line, and the EW and FWHM are computed from the best-fitted component. Our final selection criterion of N-rich quasars is  $\text{EW} > 3 \text{ \AA}$ .

<sup>1</sup> Steward Observatory, University of Arizona, Tucson, AZ 85721

<sup>2</sup> Department of Physics and Astronomy, Tufts University, Medford, MA 02155

This cut is chosen for the following reasons: (1) In most quasar spectra, the significance of the detection of a  $EW = 3 \text{ \AA}$  nitrogen line is greater than  $5\sigma$ ; (2) The  $3 \text{ \AA}$  cut is significantly larger than typical  $EW$  values for the two nitrogen lines (see § 3.2); (3) Bentz et al. (2004) used a similar selection cut. A total of 293 quasars in our sample meet this criterion, including 43 quasars with strong N IV] lines and 279 quasars with strong N III] lines (29 quasars have both lines). Table 1 presents the catalog of the N-rich quasars. Column (1) gives the name of each quasar, and column (2) lists the redshift. Column (3) shows the SDSS  $i$ -band magnitude corrected for Galactic extinction. All other quantities will be explained in § 3. The full Table 1 appears in the electronic edition of the *Astrophysical Journal*.

Figure 1 shows four good examples of the selected quasars. Figure 2 shows the rest-frame  $EW$  and  $FWHM$  distributions of N III]. Figure 3 compares the redshift distributions of the N-rich quasars and SDSS DR5 quasars at  $z > 1.7$ . The distributions are consistent at most redshift ranges except for the ranges of  $2.5 < z < 2.9$  and  $z > 3.5$ . At  $2.5 < z < 2.9$ , the higher fraction of the N-rich quasars is caused by the higher SDSS quasar selection efficiency due to stronger Ly $\alpha$  emission in these quasars (§ 3.2). The lower fraction of the N-rich quasars at  $z > 3.5$  is likely due to the lower signal-to-noise ratios (SNRs) of the spectra at  $\lambda \geq 8000 \text{ \AA}$ .

### 3. RESULTS

We detect 293 quasars with prominent N IV] or N III] emission lines from 25,941 SDSS quasars at  $1.7 < z < 4.0$ . This is the largest N-rich quasar sample to date. The fraction of N-rich quasars is about 1.1%, significantly higher than 0.4% (20 out of 5600) found by Bentz et al. (2004), who used a similar  $EW$  selection cut in a similar redshift range. This is likely because detecting weak lines in spectra of moderate SNRs is difficult for automated codes. Based on repeated selections of N-rich quasars by visual inspection from a subset of 2000 quasars, we estimate that the completeness at  $EW > 3 \text{ \AA}$  is greater than 80%. In this section we compare various properties of the N-rich quasars with those of ‘normal’ SDSS quasars.

#### 3.1. Continuum and Emission Line Properties of N-rich Quasars

To analyze the emission line properties of each N-rich quasar, we fit a power-law ( $f_\nu \propto \nu^\alpha$ ) to regions with very little contribution from line emission. The quasar spectrum was first scaled to its  $r$ -band magnitude and thereby placed on an absolute flux scale. After fitting and subtraction of the power-law continuum, we fit the following individual emission lines. (1) Si IV  $\lambda 1396$  if  $i < 19.0$  and  $z > 1.9$ . We use a single Gaussian profile to fit this line. (2) C IV if  $i < 19.5$ . We use a single Gaussian and double Gaussians to fit this line respectively, and we choose the best fit. (3) C III] if  $i < 19.5$  and  $z < 3.5$ . The weak Al III  $\lambda 1857$  line is often detected in the blue wing of the C III] line. We use two Gaussian profiles to fit these two lines simultaneously if Al III is apparent, otherwise C III] is fitted using a single Gaussian component. We also note that there is usually a contamination from the weak Si III]  $\lambda 1892$  line. We do not remove this contamination because the decomposition of the C III] and Si III] lines is difficult and the strength of Si III] is minor

compared to C III]. All models are visually inspected, and the emission lines severely affected by absorption lines are discarded from our analysis. The  $EW$  and  $FWHM$  are measured from the best fits. The results are shown in Table 1. Column 2 of Table 2 lists the median values of  $EW$  and  $FWHM$  for each line. The median value of the power-law slopes is also given in Table 2. The slope is slightly redder than the slope in the Vanden Berk et al. (2001) composite spectrum ( $\alpha_\nu = -0.44$ ). In most cases the spectral quality is not good enough to allow more sophisticated fittings as Baldwin et al. (2003) and Dhanda et al. (2007) did, or to allow reliable modeling of weak emission lines such as He II  $\lambda 1640$  and O III]  $\lambda 1663$ . The Ly $\alpha$ , N V, and Si II  $\lambda 1262$  lines are usually heavily blended, so modeling their profiles requires high quality spectra. We discuss their average properties in § 3.2.

In the above analysis we do not consider the UV Fe II emission that contaminates most of the UV spectral region. The most prominent Fe II emission line complex is at  $2200 \text{ \AA} \lesssim \lambda \lesssim 3000 \text{ \AA}$  (Vestergaard & Wilkes 2001). At  $\lambda < 2200 \text{ \AA}$ , the Fe II emission is weak, and does not significantly affect the measurements of strong emission lines. At  $z > 2.1$ , the strong Fe II complex is moving out of the SDSS spectral coverage, making it difficult to measure the Fe II emission. However, Fe abundance is of interest, and the Fe II/Mg II  $\lambda 2800$  ratio is important for understanding chemical abundances in quasars (e.g. Hamann & Ferland 1999; Dietrich et al. 2002). We fit and measure the Fe II emission for quasars with  $i < 19.0$  and  $z < 2.1$ . The modeling is done as an iteration over a power-law fit to the continuum emission and a model fit to the Fe II emission using a scaled and broadened version of the Fe II template of Vestergaard & Wilkes (2001). The Fe II template is broadened by convolving the template with Gaussians with a range of sigmas. In the first iteration a power-law is fitted to the continuum windows. Upon subtraction of this primary continuum fit multiple broadened copies of the Fe II template are scaled to regions which predominantly contain Fe emission. The broadened and scaled Fe II template that provides the best fit is selected and subtracted. Then another power-law fit to the continuum emission is performed. The iteration of the continuum and Fe II fitting is repeated until convergence is obtained. See Vestergaard & Wilkes (2001) for the detailed process. All models are visually inspected, and poor fits (due to low SNRs or strong absorptions) are discarded from our analysis.

After the subtraction of the Fe II emission and power-law continuum we fit the Mg II line using a Gaussian profile and measure its  $EW$  and  $FWHM$  from the best fit. We calculate the flux of the Fe II complex by integrating the best-fitting Fe II template from 2200 to 3090  $\text{\AA}$  (e.g. Dietrich et al. 2002). The results are shown in Table 1, and their mean values are shown in Table 2. The mean value of the Fe II/Mg II ratios is 3.6 with a scatter 1.3, consistent with previous measurements in normal quasars (e.g. Iwamuro et al. 2002).

#### 3.2. Comparison Between N-rich Quasars and ‘Normal’ Quasars

To find differences between N-rich quasars and ‘normal’ quasars, we draw a quasar sample three times larger than the sample of the N-rich quasars from the SDSS DR5 quasar catalog by random selection. The sample

has *i*-band magnitudes brighter than 20.1 and redshift distribution similar to that of the N-rich sample shown in Figure 3. We measure continuum and emission line properties for this sample using the methods outlined in § 3.1. The results are given in Column 3 of Table 2. The comparison in Table 2 shows that most of the properties in the two samples are very consistent, including the continuum slopes, the Fe II/Mg II ratios, and the EWs and FWHM of most emission lines. The only apparent difference is the FWHM of C IV and C III]; their values in the N-rich sample is about 25–30% smaller than those in the SDSS DR5 sample. This was also noticed by Bentz et al. (2004).

We compare the luminosity distributions of the two quasar samples. We measure  $m_{2500}$ , the apparent AB magnitude at rest-frame 2500 Å, based on  $m_{2500} = -2.5 \times \log(f_{2500}) - 48.60$ , where  $f_{2500}$  is the monochromatic flux density (in units of  $\text{erg sec}^{-1} \text{cm}^{-2} \text{Hz}^{-1}$ ) at rest-frame 2500 Å. The flux density  $f_{2500}$  is derived using the best-fitted continuum. We then determine the absolute magnitude  $M_{2500}$  from  $m_{2500}$ . We find that the distributions of  $M_{2500}$  for the two samples are similar, although the N-rich sample is about 0.5 magnitude brighter on average. This is caused by our selection; we may have missed some faint N-rich quasars where SNRs are low and nitrogen lines are difficult to identify. However, the difference of 0.5 magnitude is too small for the Baldwin effect (Baldwin 1977) to impact the comparison of the EWs.

To compare the overall properties of continua and emission lines, we construct composite spectra for the two samples. Each spectrum is placed in the rest frame and scaled so that its continuum at 1450 Å is equal to 1 (arbitrary units). The scaled spectra are then averaged without any weights. This is to avoid bias introduced by the Baldwin effect if we use weights involving SNRs. The two composite spectra are shown in Figure 4. They have similar shapes from 1000 to 3000 Å. By definition the N IV] and N III] lines in the N-rich spectrum are stronger. In the SDSS DR5 spectrum, the EWs of N III] is  $0.40 \pm 0.06$  Å, consistent with  $0.44 \pm 0.03$  Å in the Vanden Berk et al. (2001) composite spectrum; the EWs of N IV] is  $-0.04 \pm 0.06$  Å, consistent with no detection. We measure the properties of Ly $\alpha$  and N V as follows. After the subtraction of the power-law continuum, we fit the Ly $\alpha$ , N V, and Si II lines simultaneously using four Gaussian profiles, with the first two profiles representing the broad and narrow components of Ly $\alpha$  and the last two profiles representing N V and Si II. For Ly $\alpha$ , we only fit its red half side and mirror the fit around the peak for the EW and FWHM measurements. The EWs and FWHM for the lines are determined using the methods described in § 3.1. The results are shown in Table 2. Errors in these measurements are negligible owing to the high SNRs of the composite spectra. Compared to normal quasars, the N-rich quasars have  $\sim 40\%$  stronger Ly $\alpha$  and N V emission, and  $\sim 100\%$  stronger O I  $\lambda 1304$  emission. Their C IV and C III] line widths are 20–25% smaller, as we find in § 3.1.

The radio-loud fraction (RLF) of optically-selected quasars is a strong function of redshift and optical luminosity. We calculate the RLF for our N-rich sample following Jiang et al. (2007). Radio loudness  $R$  is defined

by  $R = f_{6cm}/f_{2500}$ , where  $f_{6cm}$  is the observed flux density at rest-frame 6 cm derived from FIRST (if detected) assuming a power-law slope of  $-0.5$ . When quasars with  $R > 10$  are defined as radio-loud, FIRST is able to detect radio-loud quasars down to  $i \approx 18.9$  (Jiang et al. 2007). We find that the RLF in the N III]-rich quasars is 26% and in the N IV]-rich quasars is 69%. The RLF in quasars with both N IV] and N III] lines even reaches 80%, significantly higher than the RLF  $\sim 8\%$  found in normal SDSS quasars with similar redshift and luminosity (Jiang et al. 2007). This suggests that the N IV] and N III] emission in these quasars are related to the quasar radio properties.

Central black hole masses of quasars can be estimated using mass scaling relations based on broad emission line widths and continuum luminosities. The scaling relations are written as  $M_{\text{BH}} \propto \text{FWHM}^2 L_{\text{opt}}^\beta$ , where  $L_{\text{opt}}$  is optical luminosity and  $\beta \approx 0.5$ . Strong emission lines such as Mg II and C IV have been widely used to determine black hole masses (e.g. McLure & Dunlop 2004; Vestergaard & Peterson 2006; Shen et al. 2007). Based on the similar luminosities and FWHM of Mg II in Table 2, the black hole masses in the two quasar subsets are consistent.

Photoionization models have shown that a series of emission-line ratios can be used to estimate gas metallicity in the broad line region of quasars (Hamann et al. 2002; Nagao et al. 2006). In particular, the relative nitrogen abundance is a good metallicity indicator if it serves as a secondary element so that  $\text{N/O} \propto \text{O/H}$ . By definition, N-rich quasars have much stronger N IV] or N III] emission. They also have stronger Ly $\alpha$  and N V emission. Since N V, N IV], and N III] have a range of critical densities and ionization parameters, stronger N V, N IV], and N III] emission shows higher nitrogen abundance, and higher metallicities if the relation  $\text{N/O} \propto \text{O/H}$  holds in these quasars. For example, a  $\sim 40\%$  stronger N V/C IV ratio in N-rich quasars in Table 2 indicates a  $\sim 40\%$  higher metallicity according to Hamann et al. (2002). However, the strengths of most other emission lines in N-rich quasars are similar to those in normal quasars, and thus the metallicities measured from line ratios other than nitrogen (Nagao et al. 2006) would be consistent for the two samples, which is contrary to the results from nitrogen. Therefore, stronger N V, N IV], and N III] emission in N-rich quasars may not indicate a higher overall metallicity; instead, it simply means a larger nitrogen abundance. The nitrogen enrichment in these quasars could significantly deviate from the usual  $\text{N/O} \propto \text{O/H}$  scaling.

#### 4. SUMMARY

We have obtained a sample of 293 SDSS quasars with strong N IV] or N III] emission lines at  $z > 1.7$ . The fraction of N-rich quasars is about 1.1%. The comparison between these N-rich quasars and normal quasars shows that the two quasar subsets have similar: (1) redshift and luminosity distributions; (2) UV continuum slopes; (3) line strengths and widths for most emission lines; and (4) central black hole masses. However, the N-rich quasars have: (1)  $\sim 40\%$  stronger Ly $\alpha$  and N V emission. Strong nitrogen emission in all ionization states indicates high overall nitrogen abundances. (2) 20–25% narrower widths of the C IV and C III] lines; and (3) a much higher RLF. Almost all the quasars with both N IV] and N III]

lines are radio-loud.

The most intriguing difference between the two quasar subsets is the much higher RLF of N-rich quasars. We notice that Q0353-383 is also a radio-loud quasar with  $R \approx 130$  based on the optical observation of Osmer & Smith (1980) and the radio observation of Condon et al. (1998). Also the N IV] and N III] lines are rarely seen in normal galaxies, but they seem more common in luminous radio galaxies with AGN signatures. For example, the two lines were detected at  $\geq 5\sigma$  significance in 67% radio galaxies in the sample of Vernet et al. (2001). All these results indicate that the nitrogen abundance is tightly related to quasar radio properties: perhaps the high nitrogen abundance in N-rich quasars is an indicator of a special quasar evolution stage, in which the radio activity is also very strong. Detailed models, which are beyond the scope of this letter, have to explain all the distinguishing features of N-rich quasars found in this work.

We acknowledge support from NSF grant AST-0307384, a Sloan Research Fellowship and a Packard Fellowship for Science and Engineering (LJ, XF). We thank F. Hamann, C. Tremonti and D. Zaritsky for helpful discussions.

Funding for the SDSS and SDSS-II has been provided by the Alfred P. Sloan Foundation, the Participating Institutions, the National Science Foundation, the U.S. Department of Energy, the National Aeronautics and Space Administration, the Japanese Monbukagakusho, the Max Planck Society, and the Higher Education Funding Council for England. The SDSS is managed by the Astrophysical Research Consortium for the Participating Institutions. The SDSS Web Site is <http://www.sdss.org/>.

#### REFERENCES

- Baldwin, J. A. 1977, *ApJ*, 214, 679  
 Baldwin, J. A., Hamann, F., Korista, K. T., Ferland, G. J., Dietrich, M., & Warner, C. 2003, *ApJ*, 583, 649  
 Becker, R. H., White, R. L., & Helfand, D. J. 1995, *ApJ*, 450, 559  
 Bentz, M. C., Hall, P. B., & Osmer, P. S. 2004, *AJ*, 128, 561  
 Condon, J. J., Cotton, W. D., Greisen, E. W., Yin, Q. F., Perley, R. A., Taylor, G. B., & Broderick, J. J. 1998, *AJ*, 115, 1693  
 Dhanda, N., Baldwin, J. A., Bentz, M. C., & Osmer, P. S. 2007, *ApJ*, 658, 804  
 Dietrich, M., Appenzeller, I., Vestergaard, M., & Wagner, S. J. 2002, *ApJ*, 564, 581  
 Fukugita, M., Ichikawa, T., Gunn, J. E., Doi, M., Shimasaku, K., & Schneider, D. P. 1996, *AJ*, 111, 1748  
 Glikman, E., Djorgovski, S. G., Stern, D., Bogosavljević, M., & Mahabal, A. 2007, *ApJ*, 663, L73  
 Gunn, J. E., et al. 2006, *AJ*, 131, 2332  
 Hamann, F., & Ferland, G. 1999, *ARA&A*, 37, 487  
 Hamann, F., Korista, K. T., Ferland, G. J., Warner, C., & Baldwin, J. 2002, *ApJ*, 564, 592  
 Iwamuro, F., Motohara, K., Maihara, T., Kimura, M., Yoshii, Y., & Doi, M. 2002, *ApJ*, 565, 63  
 Jiang, L., Fan, X., Ivezić, Ž., Richards, G. T., Schneider, D. P., Strauss, M. A., & Kelly, B. C. 2007, *ApJ*, 656, 680  
 McLure, R. J., & Dunlop, J. S. 2004, *MNRAS*, 352, 1390  
 Nagao, T., Marconi, A., & Maiolino, R. 2006, *A&A*, 447, 157  
 Osmer, P. S., & Smith, M. G. 1980, *ApJS*, 42, 333  
 Richards, G. T., et al. 2002, *AJ*, 123, 2945  
 Schneider, D. P., et al. 2003, *AJ*, 126, 2579  
 Schneider, D. P., et al. 2007, *AJ*, 134, 102  
 Shen, Y., Greene, J. E., Strauss, M. A., Richards, G. T., & Schneider, D. P. 2007, *ApJ*, submitted (astro-ph/0709.3098)  
 Spergel, D. N., et al. 2007, *ApJS*, 170, 377  
 Vanden Berk, D. E., et al. 2001, *AJ*, 122, 549  
 Vernet, J., Fosbury, R. A. E., Villar-Martín, M., Cohen, M. H., Cimatti, A., di Serego Alighieri, S., & Goodrich, R. W. 2001, *A&A*, 366, 7  
 Vestergaard, M. & Wilkes, B. J. 2001, *ApJS*, 134, 1  
 Vestergaard, M., & Peterson, B. M. 2006, *ApJ*, 641, 689  
 York, D. G., et al. 2000, *AJ*, 120, 1579

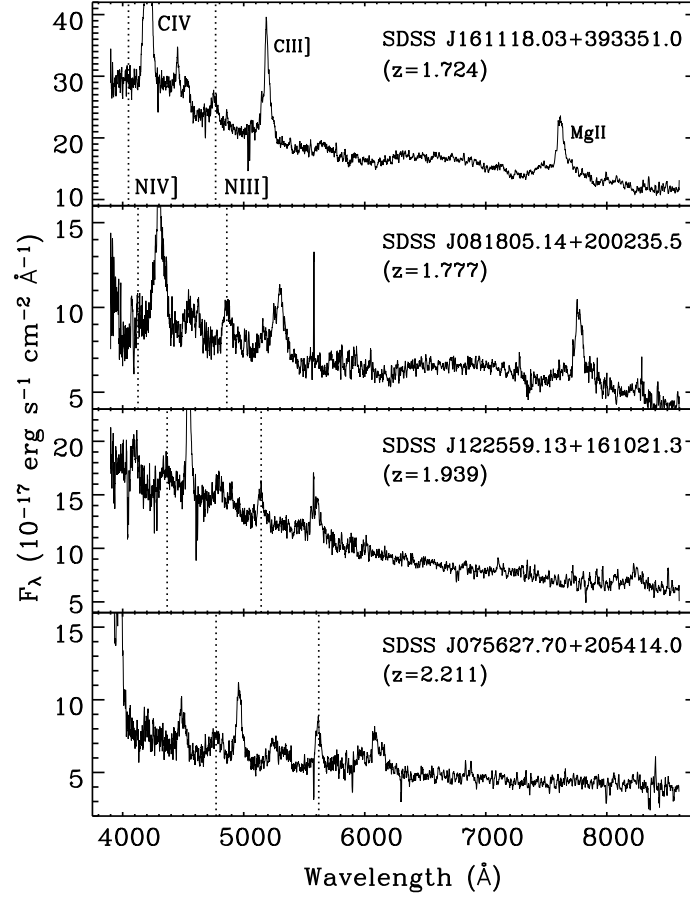


FIG. 1.— Spectra of four N-rich quasars, smoothed by a boxcar of 5 pixels. The dotted lines indicate the positions of N IV] and N III]. The first two quasars show strong N III] lines and the last two quasars show both N IV] and N III] lines.

TABLE 1  
SDSS DR5 N-RICH QUASAR CATALOG

| Name (J2000.0 Coordinates) | Redshift | $i^a$ | $\alpha$ | EW (Å) |        |       |       |        |       | Fe II/Mg II | $M_{2500}$ | $R$    |
|----------------------------|----------|-------|----------|--------|--------|-------|-------|--------|-------|-------------|------------|--------|
|                            |          |       |          | N IV]  | N III] | Si IV | C IV  | C III] | Mg II |             |            |        |
| SDSS J124032.96+674810.8   | 1.701    | 18.91 | -0.63    | ...    | 4.0    | ...   | 27.1  | 31.2   | 11.4  | 4.2         | -25.27     | ...    |
| SDSS J082247.75+071154.7   | 1.703    | 18.85 | -0.46    | ...    | 5.3    | ...   | 35.6  | 27.1   | 14.6  | 2.5         | -25.30     | ...    |
| SDSS J100643.89+395222.7   | 1.705    | 18.89 | -0.85    | ...    | 4.2    | ...   | 101.7 | 22.8   | ...   | ...         | -25.26     | ...    |
| SDSS J141000.79+641010.4   | 1.707    | 18.46 | -1.15    | ...    | 4.1    | ...   | ...   | 37.4   | 21.8  | 3.1         | -25.66     | ...    |
| SDSS J105645.42+414016.2   | 1.708    | 18.71 | -0.32    | ...    | 3.0    | ...   | 26.6  | 20.5   | 7.8   | 4.4         | -25.48     | ...    |
| SDSS J105743.11+532231.4   | 1.708    | 18.52 | -0.57    | ...    | 3.4    | ...   | 41.0  | 21.2   | 15.9  | 2.4         | -25.70     | ...    |
| SDSS J075230.44+272619.8   | 1.708    | 18.25 | -0.62    | ...    | 3.3    | ...   | 67.2  | 41.4   | 24.4  | 1.8         | -25.87     | ...    |
| SDSS J151557.86+383604.3   | 1.710    | 18.24 | -0.94    | ...    | 3.6    | ...   | ...   | 45.2   | 16.9  | 2.9         | -25.96     | ...    |
| SDSS J115419.40+145555.3   | 1.711    | 17.98 | -0.87    | ...    | 3.6    | ...   | ...   | 15.9   | ...   | ...         | -26.30     | ...    |
| SDSS J162923.06+462311.2   | 1.718    | 18.95 | -0.39    | ...    | 3.2    | ...   | 43.6  | 28.8   | 13.8  | 2.9         | -25.28     | ...    |
| SDSS J145349.70+482740.3   | 1.720    | 18.81 | -1.07    | ...    | 5.1    | ...   | 19.9  | 20.6   | ...   | ...         | -25.52     | 232.6  |
| SDSS J074220.27+343213.3   | 1.724    | 19.77 | -0.92    | ...    | 4.8    | ...   | ...   | ...    | ...   | ...         | -24.41     | 71.4   |
| SDSS J161118.02+393350.9   | 1.724    | 17.82 | -0.57    | ...    | 3.9    | ...   | 30.9  | 16.6   | ...   | ...         | -26.38     | 4.3    |
| SDSS J081710.54+235223.9   | 1.732    | 18.61 | -0.40    | 4.9    | 6.7    | ...   | 8.1   | 13.7   | ...   | ...         | -25.58     | 1901.2 |
| SDSS J145958.75-013742.4   | 1.738    | 18.84 | -1.44    | ...    | 6.9    | ...   | ...   | 45.1   | ...   | ...         | -25.35     | ...    |
| SDSS J084057.02+054733.4   | 1.742    | 18.15 | -1.50    | ...    | 4.3    | ...   | 24.4  | 24.3   | ...   | ...         | -26.25     | ...    |
| SDSS J123354.39+150203.7   | 1.744    | 18.13 | -1.29    | ...    | 5.1    | ...   | 34.3  | 22.8   | 15.2  | 2.5         | -26.18     | ...    |
| SDSS J084117.24+083753.4   | 1.746    | 18.11 | -1.04    | ...    | 5.6    | ...   | 39.8  | 26.5   | 15.6  | 2.7         | -26.17     | ...    |
| SDSS J111559.52+633813.6   | 1.746    | 18.04 | -1.12    | ...    | 3.4    | ...   | 46.5  | 25.3   | ...   | ...         | -26.15     | 22.7   |
| SDSS J231608.20+132334.5   | 1.748    | 18.42 | -1.23    | ...    | 9.1    | ...   | 52.6  | 27.5   | ...   | ...         | -25.84     | ...    |

NOTE. — The full Table 1 appears in the electronic edition of the *Astrophysical Journal*.

<sup>a</sup> Corrected for Galactic extinction.

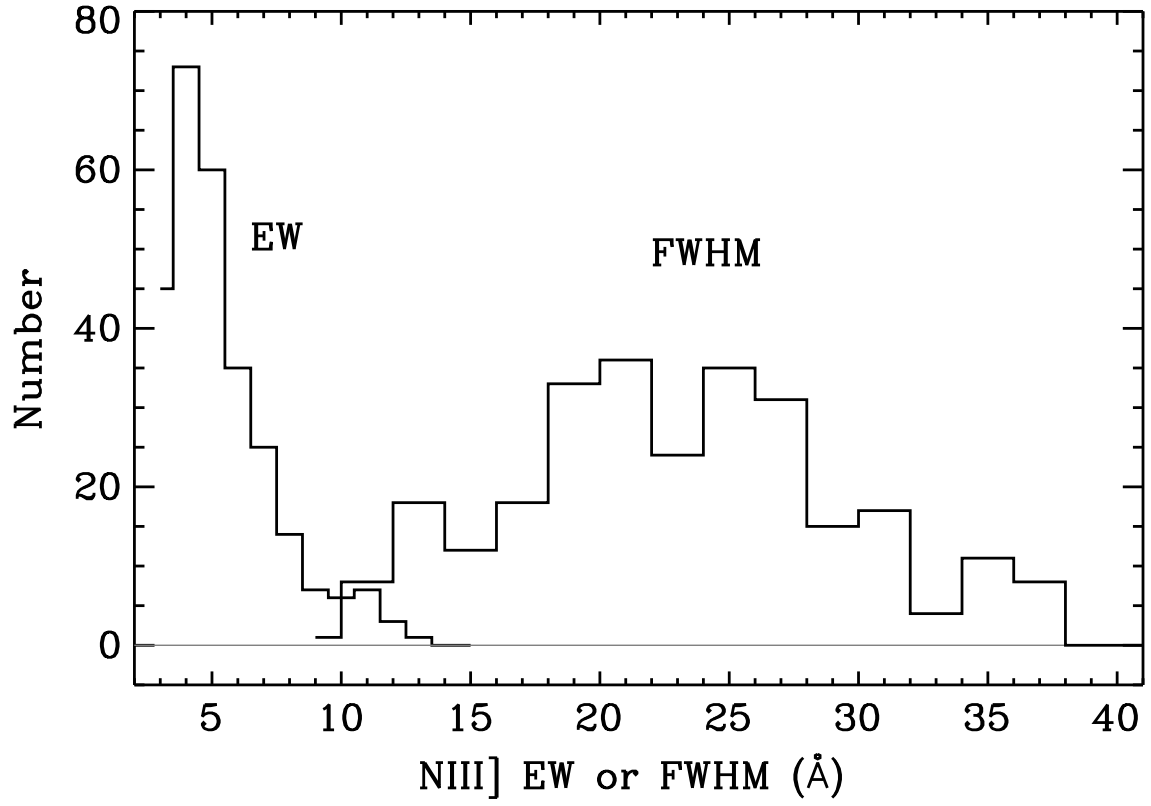


FIG. 2.— Rest-frame EW and FWHM distributions of N III].

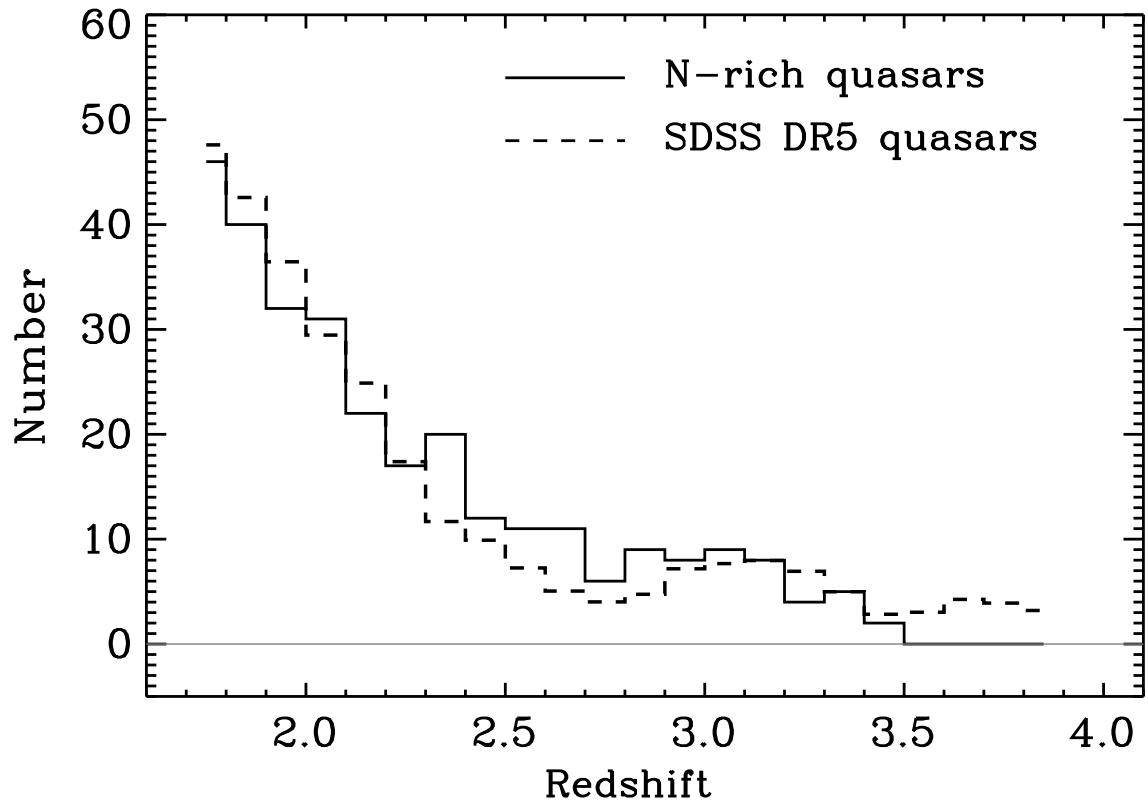


FIG. 3.— Redshift distributions of the N-rich quasars and SDSS DR5 quasars. The histogram for the SDSS DR5 quasars has been scaled to match the number of the N-rich quasars.

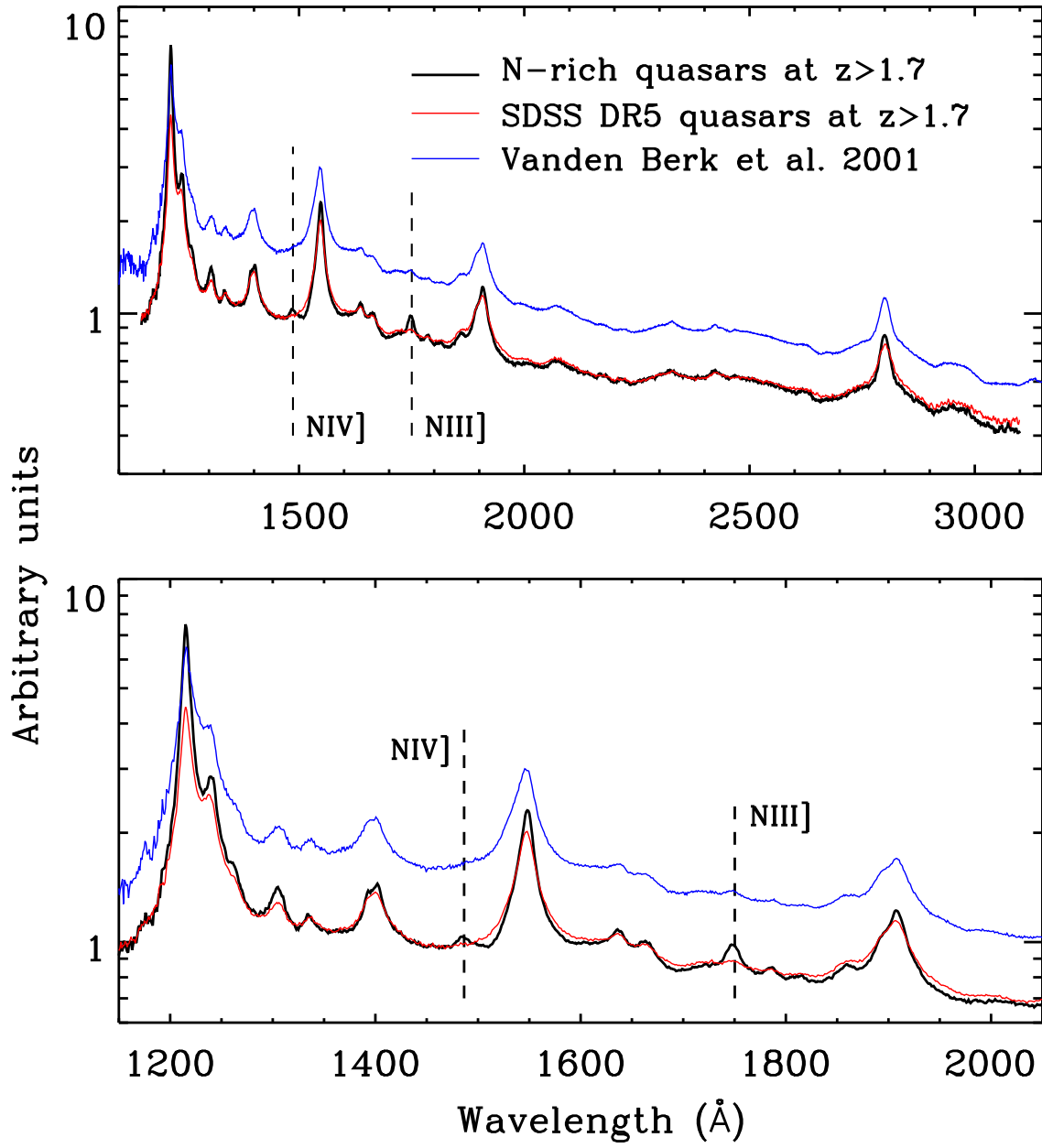


FIG. 4.— Composite spectra for the N-rich quasars (black) and SDSS DR5 quasars (red) at  $z > 1.7$ . The dashed lines indicate the positions of  $\text{N IV]}$  and  $\text{N III]}$ . For comparison, the blue lines show the composite spectrum of Vanden Berk et al. (2001).

TABLE 2  
REST-FRAME EMISSION LINE PROPERTIES

| Parameter                         | N-rich quasars   | SDSS quasars     |
|-----------------------------------|------------------|------------------|
| $\alpha$                          | $-0.68 \pm 0.40$ | $-0.64 \pm 0.57$ |
| Si IV EW (Å)                      | $8.1 \pm 3.3$    | $8.1 \pm 3.4$    |
| Si IV FWHM (Å)                    | $22.9 \pm 5.4$   | $26.3 \pm 8.3$   |
| C IV EW (Å)                       | $36.9 \pm 16.6$  | $36.1 \pm 19.7$  |
| C IV FWHM (Å)                     | $18.9 \pm 8.7$   | $27.9 \pm 11.0$  |
| C III] EW (Å)                     | $21.8 \pm 9.4$   | $23.8 \pm 9.0$   |
| C III] FWHM (Å)                   | $37.2 \pm 14.9$  | $50.5 \pm 21.0$  |
| Mg II EW (Å)                      | $13.7 \pm 5.0$   | $11.1 \pm 4.6$   |
| Mg II FWHM (Å)                    | $41.6 \pm 7.8$   | $43.1 \pm 12.0$  |
| Fe II/Mg II                       | $3.6 \pm 1.3$    | $3.5 \pm 1.4$    |
| <sup>a</sup> Ly $\alpha$ EW (Å)   | 71.0             | 50.0             |
| <sup>a</sup> Ly $\alpha$ FWHM (Å) | 10.6             | 15.8             |
| <sup>a</sup> N V EW (Å)           | 24.6             | 17.8             |
| <sup>a</sup> N V FWHM (Å)         | 18.0             | 19.0             |
| <sup>a</sup> O I EW (Å)           | 3.7              | 1.8              |
| <sup>a</sup> O I FWHM (Å)         | 14.8             | 14.1             |
| <sup>a</sup> C IV EW (Å)          | 38.4             | 39.6             |
| <sup>a</sup> C IV FWHM (Å)        | 18.6             | 24.0             |
| <sup>a</sup> C III] EW (Å)        | 23.4             | 24.9             |
| <sup>a</sup> C III] FWHM (Å)      | 35.1             | 44.9             |

NOTE. — The errors are  $1\sigma$  rms of the distributions.  
<sup>a</sup> Derived from the composite spectra in § 3.2.